ACS OMEGA

Open Access

http://pubs.acs.org/journal/acsodf

Article

Multifunctional Carbon Nanodots for Antibacterial Enhancement, pH Change, and Poisonous Tin(IV) Specifical Detection

Yingnan Jiang,[‖] Xinyu Zhao,[‖] Xuechun Zhou, Xiaoyu He, Zhe Zhang,* Lizhi Xiao, Jing Bai, Ying Yang, Lei Zhao,* Yu Zhao,* and Quan Lin

Cite This: *ACS Omega* 2023, 8, 41469−41479

Read Online

ACCESS | Metrics & More | Article Recommendations | Supporting Information

ABSTRACT: In recent years, antibiotic-based carbon nanodots have been extensively developed and studied, because of their excellent synergistic fluorescence and antibacterial properties. These antibacterial carbon nanodots have also been developed with various new applications, such as heavy iron detection, pH sensitivity, temperature response, and bacterial count detection in various environments. In this article, using vancomycin hydrochloride as the only precursor, vancomycin hydrochloride carbon nanodots were rapidly synthesized by a one-step microwave method. The diameter of the vancomycin hydrochloride carbon nanodots was concentrated at 0.899 ± 0.40 nm with a uniform size and excitation-dependent fluorescence. Vancomycin hydrochloride carbon nanodots showed better antibacterial activity than the original vancomycin hydrochloride with low biological toxicity and good stability. In the pH range of approximately 7−13, there was a good linear relationship between the fluorescence intensity of the carbon nanodots and the pH value (R^2 = 0.98516). Moreover, vancomycin hydrochloride carbon nanodots could quickly and specifically detect poisonous Sn^{4+} through changes in their fluorescence intensity, with a detection limit of approximately 5.2 μM. Multifunctional vancomycin hydrochloride carbon nanodots have good application prospects in the fields of antibacterial, toxic Sn^{4+} detection, and pH-sensitive aspects.

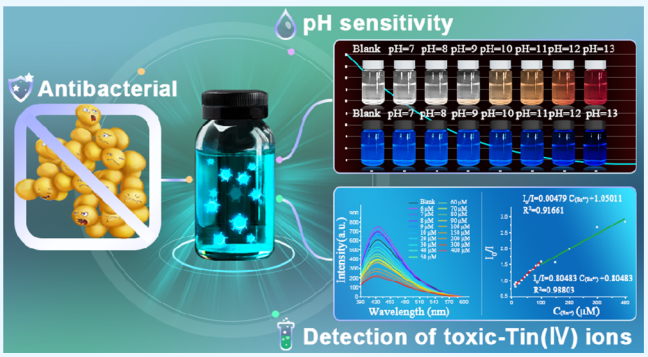

1. INTRODUCTION

Carbon nanodots (CDs) have attracted considerable attention because of their excellent fluorescence properties, water solubility, biocompatibility, and low toxicity.[1−6] Based on their excellent performance, CDs have been widely explored in various fields, including in biomedical imaging and sensing, as drug carriers, and antibacterial drugs.[7−12] Numerous CDs with antibacterial activity have been fabricated, including a series of carbon quantum dots (CQDs) derived from gentamicin, which were calcined at different temperatures and whose antibacterial activity indicated their superiority to the original gentamicin (Li et al.).[13] Among them, CQD180 demonstrated optimal characteristics of high efficiency and low resistance to bacterioplankton as well as the ability to destroy the established biofilm of *Staphylococcus aureus* with no detectable toxicity to mammalian cells. Li et al. also found that the antimicrobial activity of the prepared CQDs was superior to that of progentamicin owing to their dual antimicrobial mode using surface positive charge and reactive oxygen species generation, with good inhibitory effects on all eight types of bacteria tested. Moreover, Luo et al. synthesized novel carbon dots (CDs Kan) using the broad-spectrum antibiotic kanamycin sulfate through a one-step hydrothermal method.[14] CDs Kan retained the main bactericidal functional groups and antibacterial activity of Kan and had a good inhibitory effect on Gram-negative *Escherichia coli* and Gram-positive *S. aureus*. Notably, many studies on antibacterial CDs have used antibiotics as reaction precursors. Moreover, it has been claimed that the synthesized CDs retain a portion of the active structure of the original drug, thus possessing similar antibacterial properties.[15] We previously used cefminox sodium (CS) as the sole precursor to synthesize cefminox sodium carbon nanodots (CS-CDs) via a rapid one-step microwave method.[16] CS-CDs can rapidly and quantitatively detect the number of *E. coli* in the blood while effectively treating bloodstream infections. We proved that both CS-CDs and CS drugs acted similarly on bacterial cell walls, mainly on the growth process of bacteria (e.g., inhibiting cell wall synthesis and interfering with the synthesis of important proteins, DNA, and RNA), to achieve antibacterial effects. As a result, both the bacterial walls and membranes are obviously ruptured, leading to the leakage of intracellular substances.

Received: July 22, 2023
Accepted: October 4, 2023
Published: October 23, 2023

https://doi.org/10.1021/acsomega.3c05319
ACS Omega 2023, 8, 41469−41479

Scheme 1. Synthetic Route of VAN-CDs and Their Application for Antibacterial Activity and pH Sensitivity as well as Detecting the Poisonous Sn^{4+} Quickly and Specifically

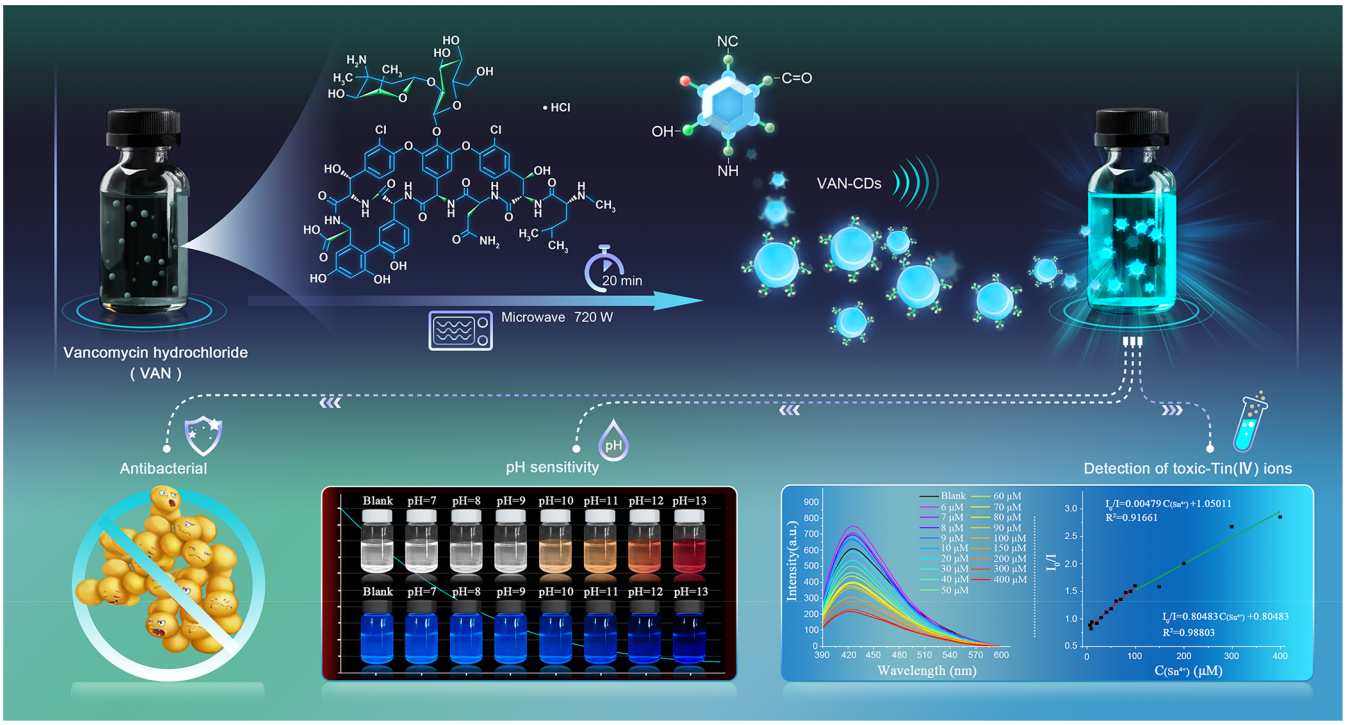

Due to their excellent synergistic fluorescence and antibacterial properties, antibiotic-based carbon nanodots have also been extensively developed and studied with various new applications, including heavy iron detection, pH sensitivity, temperature response, and bacterial count detection in various environments. Monitoring pH is crucial for scientific research and practical applications in many fields such as disease diagnosis, environmental examination, and food analysis. Nanomaterials, including CDs with a tunable response range and strong fluorescence signals, are considered to be some of the most promising materials for pH sensors. For example, Zhu et al. demonstrated that double-doped CQDs had good pH sensitivity and ion doping properties.[17] Lipid/double-doped CQDs could be used to reveal the drug release rates of liposomes at different pH values and demonstrate potential antitumor therapeutic effects *in vivo*. Sun et al. prepared CDs doped with silicon for use as pH-sensitive fluorescent inks for information encryption.[18] Yang et al. synthesized novel pH-sensitive carbon dots (O-CDs) using 1,2,4-triaminobenzene and urea in aqueous solutions via a microwave-assisted method.[19] O-CDs exhibit excellent pH sensitivity in their photoluminescence (PL) intensity, but they also exhibited a colorimetric response to pH changes from 5 to 9 under visible light.

Many metal ions have high chemical toxicity and are widely present in the atmosphere, water, and soil; these metal ions can migrate through the food chain, accumulate in the human body, and cause serious harm. Notably, because of the abundant functional groups on the surface, CDs are prone to interacting with metal ions, leading to significant changes in their fluorescence signal. Therefore, CDs can serve as fluorescent probes to quickly and effectively detect many metal ions, with the hope of replacing traditional expensive and complex detection methods. Zong et al. synthesized CDs with large amounts of −COOH, −OH, and $-NH_2$ on the surface.[20] Quantitative detection of Cu^{2+} was achieved by quenching the fluorescence of CDs by forming a complex between Cu^{2+} and CDs. Ansi et al. prepared fluorescent probe CDs using sucrose as a carbon source to detect Pb^{2+}.[21] In the presence of Pb^{2+}, CDs exhibited significant agglomeration in water, thereby providing another method for detecting Pb^{2+}. Sun et al. synthesized strong red emission CDs using phenylenediamine as a carbon source via microwave synthesis.[22] The red fluorescence of CDs was quenched in the presence of Fe^{3+} ions. Notably, most metal ion detections have focused on common Hg, Cu, Cr, Pb, and Fe ions, while there has been little research on the detection of other metal ions such as toxic tin. Indeed, only a trace amount of Sn^{4+} can harm human health, causing symptoms such as difficulty breathing, chest tightness, diarrhea, nausea, and dizziness. Sn poisoning can also cause serious damage to liver function and nervous system. In the last two decades, with the continuous development of industry, the use and consumption of tin have been increasing annually in many fields, including electronics, information, electrical appliances, chemical industry, metallurgy, and food packaging.[23−27] However, Sn poisoning has received limited attention worldwide, with relatively few corresponding detection probes and methods. Liu et al. synthesized a fluorescent sensor, 1,4-bis(2-(quinoline-8-epoxy) acetyl) pyrazine (DQS), which had sensing ability to Sn^{4+} within the pH range of 4−10.[28] Du et al. used molybdenum oxide (MoO_3) nanomaterials to colorimetrically detect Sn^{2+} and NO_2^-.[29] However, the results induced by NO_2^- were unstable and only increased over time, thus resulting in poor analysis accuracy. To the best of our knowledge, CDs with low toxicity and stable fluorescence properties, which have been used for various metal ion detections, have not yet been applied as fluorescence probes in the detection of tin(IV). Zhu et al. synthesized compound 7-diethylamino-3-(20-(1*H*-imidazo[4,5-*b*]phenazine)yl) coumarin (DIPC) as a fluorescent probe for detecting tin(IV) ions in dimethyl sulfoxide (DMSO)−water; however, this is permeable to human skin and irritating to eyes.[30]

https://doi.org/10.1021/acsomega.3c05319
ACS Omega 2023, 8, 41469−41479

Vancomycin is a narrow-spectrum antibiotic that has strong bactericidal power but is effective only against Gram-positive bacteria. Vancomycin mainly binds to the bacterial cell wall, preventing certain amino acids from entering the glycopeptides of the bacterial cell wall and inhibiting the synthesis of bacterial cell walls.[31,32] In this study, vancomycin hydrochloride (VAN) was used as the only reactant to rapidly synthesize multifunctional vancomycin hydrochloride carbon nanodots (VAN-CDs) via a microwave method (Scheme 1). VAN-CDs with low biological toxicity showed prior antibacterial activity to the original drug and were sensitive to pH value (approximately 7−13) and Sn^{4+} concentration (limit of detection approximately 5.2 μM).

2. EXPERIMENTAL SECTION

2.1. Device. We used a Shimadzu UV-2550 ultraviolet−visible spectrophotometer to obtain UV−vis absorption spectra and a VERTEX 70 (resolution: 2 cm^{-1}, coadding times: 32 times) Fourier transform infrared spectrometer (Bruker, Germany) to obtain the infrared spectra. We used a Tecnai F20 electron microscope (FEI Company, Netherlands) to obtain transmission electron microscopy (TEM) images of VAN-CDs, and an EM-14100BINOC (JEOL Company, Japan) electron microscope with an accelerating voltage of 80 kV to obtain TEM images of VAN-CDs/VAN in *S. aureus*. We used an infinite M200 PRO (TECAN, Switzerland) to obtain fluorescence spectra and an FLS 920 steady-state/transient fluorescence spectrometer (Edinburgh, Scotland) to obtain the fluorescence lifetime and quantum yield. We used an ESCALAB 250x photoelectron spectrometer (Thermo Scientific, USA) to perform X-ray photoelectron spectroscopy.

2.2. Materials. Vancomycin hydrochloride (98%) and anhydrous tin(II) chloride (98%) were purchased from Shanghai Yuanye Bio-Technology Co., Ltd. (China). The cell counting kit-8 (CCK8) was purchased from Wuhan Boster Biological Technology Co., Ltd. Culture medium and a penicillin-streptomycin solution were purchased from VivaCell (Shanghai, China). All of the metal ion solutions were purchased from the Standard Samples Institute of the Ministry of Environmental Protection. The water used in all of the experiments was ultrapure.

2.3. Preparation of VAN-CDs. Briefly, 10 mL of VAN aqueous solution of different concentrations (0.5, 1, 2, and 5 mg/mL) was set in a 100 mL beaker and then heated in a 720 W microwave oven for 20 min. After the reaction, a 0.22 μm poly(ether sulfone) membrane was used to remove impurities. Then, the filtered solution was added to an ultrafiltration tube (10,000 MWCO) and centrifuged (5000 rpm, 5 min) twice. Finally, the yellow VAN-CDs solution was obtained and stored at 4 °C.

2.4. Bacterial Culture. *Staphylococcus aureus* (ATCC25923) was transferred from Luria−Bertani (LB) solid medium to the LB liquid medium. To reach the logarithmic growth stage, the *S. aureus* solution was cultured (200 rpm) at 37 °C for 8 h.

2.5. Distribution of VAN-CDs in *S. aureus* by TEM. *S. aureus* in the logarithmic growth phase was incubated with the same concentration (0.8 mg/mL) of VAN-CDs/VAN for 0, 2, 6, 8, and 12 h. After centrifugation, fixation, dehydration, coating, and section staining, the distribution of *S. aureus* was imaged by TEM.[33]

2.6. Cell Culture. All of the cells (MC3T3-E1, HEK 293T, LO2, and HCM) were obtained from the American-type culture collection (ATCC, Manassas, VA, U.S.) and cultured in a humidified incubator containing 5% CO_2 at 37 °C.

2.7. Inhibition Zone Test. Filter papers (diameter of approximately 6 mm) were placed in different concentrations of VAN-CDs solution overnight. *S. aureus* was coated on the LB solid medium. Each soaked paper was placed in the center of a culture plate and incubated under a constant temperature and humidity at 37 °C overnight.

2.8. Bacteriostatic Curve Test. LB medium, *S. aureus* solution, and *S. aureus* were incubated with different concentrations of VAN (10, 20, 60, and 100 μg/mL) and incubated with different concentrations of VAN-CDs (10, 20, 60, 80, and 100 μg/mL) in a 37 °C water bath constant temperature shaker. After 0, 2, 4, 6, 8, 10, 12, 24, and 48 h, 200 μL of each mixed solution was aspirated and transferred to a sterile 96-well plate. Then, the OD value of each solution was tested.

2.9. In Vitro Cytotoxicity of VAN-CDs. MC3T3-E1 cells were cultured to an appropriate cell density of 3000−5000 cells/well and then transferred to a 96-well cell culture plate and cultured for 24 h. Subsequently, 180 μL of cell suspension per well was placed in an incubator under 5% CO_2 at 37 °C until the cells were completely attached to the wall of the cell bottle. Next, 20 μL of VAN-CDs was added to each well at 0, 50, 100, 150, and 200 μg/mL. After 48 h, 20 μL of CCK-8 was added to each well and placed in the incubator for 30 min. The OD value was measured at 450 nm and was used to calculate the MC3T3-E1 cell viability.

The experimental procedures for testing the cell viability of LO2, HCM, and HEK 293T were the same as those outlined above.

2.10. Stability of the VAN-CDs. Briefly, the VAN-CDs solution (6 mg/mL) was mixed with different concentrations of NaCl/KCl solution at room temperature. The final concentrations of each mixed solution were fixed as follows: VAN-CDs at 3 mg/mL with NaCl/KCl to final concentrations of 0.1, 0.2, 0.3, 0.4, 0.5, 0.6, 0.7, 0.8, 0.9, 1.0, 1.5, and 2.0 mol/L. The fluorescence spectra of each mixed solution were determined at an excitation wavelength of 360 nm.

Next, the VAN-CDs solution (3 mg/mL) was exposed under UV irradiation at 365 nm for 10, 20, 30, 40, 50, 60, 70, 80, 90, 100, 110, 120, 130, 140, 150, 160, 170, and 180 min before the fluorescence spectra of the solution at each time point were determined at an excitation wavelength of 360 nm.

The VAN-CDs solution (3 mg/mL) was placed at −20, 4, 25, 37, 50, 60, and 70 °C for 10 min, before the fluorescence spectra of each solution were determined at an excitation wavelength of 360 nm.

2.11. pH-Sensitive Detection. A series of VAN-CDs solutions (3 mg/mL) with the same volume were adjusted to pH values of 7, 8, 9, 10, 11, 12, and 13 using NaOH. The fluorescence spectrum of each solution was measured at an excitation wavelength of 360 nm for 0, 2, 6, 24, and 48 h at room temperature. Each solution was photographed simultaneously under a 365 nm UV lamp and visible light.

2.12. Cation Sensitivity Detection. The VAN-CDs solution (6 mg/mL) was mixed with different cation solutions (Ba^{2+}, Pb^{2+}, Al^{3+}, Cr^{6+}, Ni^{2+}, Mg^{2+}, Mn^{2+}, Zn^{2+}, Cu^{2+}, Na^{+}, Fe^{2+}, K^{+}, Fe^{3+}, Cd^{2+}, Hg^{2+}, and Sn^{4+}) at room temperature. The final concentration of each mixed solution was fixed as follows: VAN-CDs at 3 mg/mL with Ba^{2+}, Pb^{2+}, Al^{3+}, Cr^{6+}, Ni^{2+}, Mg^{2+}, Mn^{2+}, Zn^{2+}, Cu^{2+}, Na^{+}, Fe^{2+}, K^{+}, Fe^{3+}, Cd^{2+}, Hg^{2+}, and Sn^{4+} to a final concentration of 100 μM. The fluorescence spectra of each

https://doi.org/10.1021/acsomega.3c05319
ACS Omega 2023, 8, 41469−41479

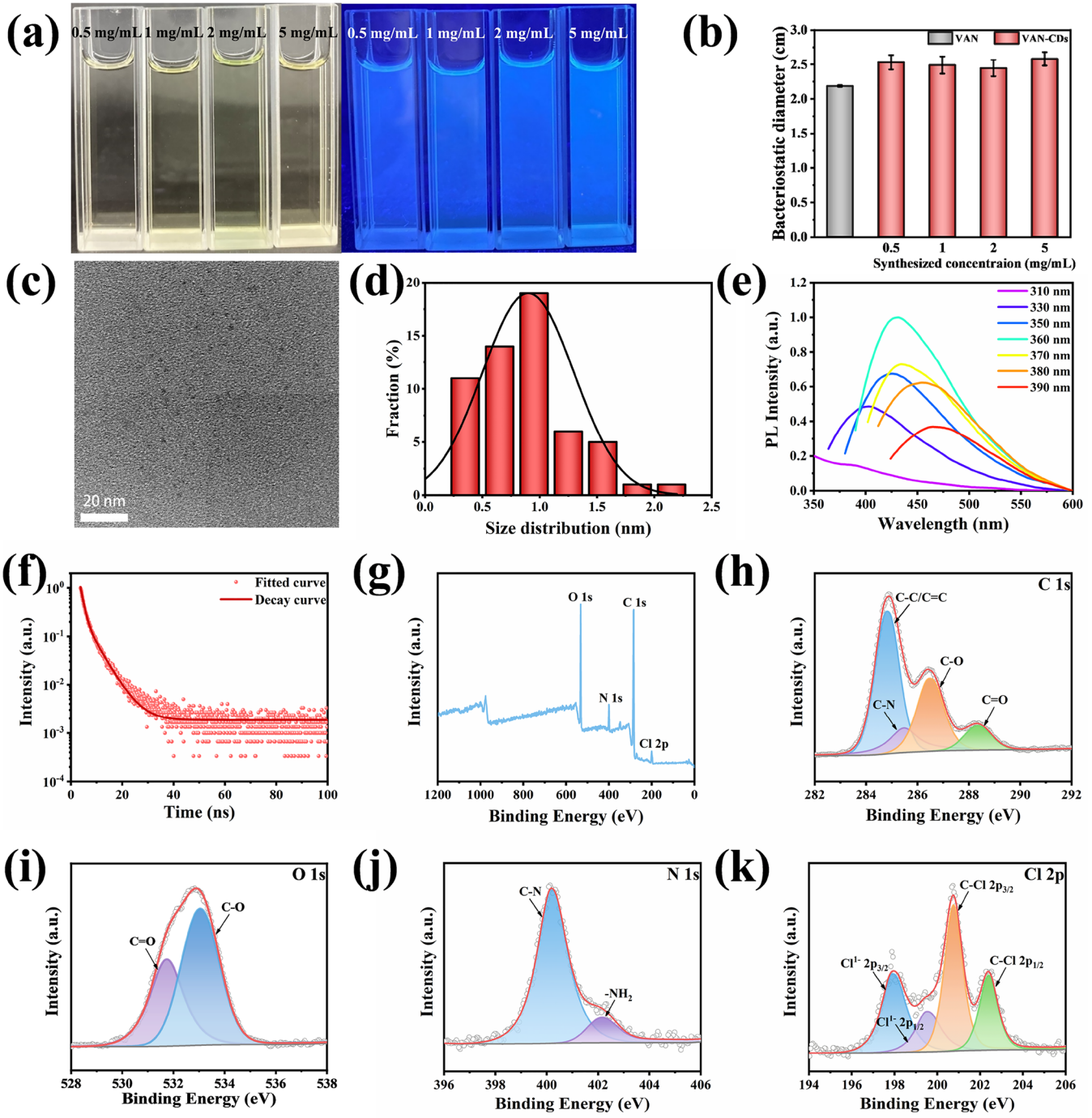

Figure 1. (a) Photos of VAN-CDs synthesized at different concentrations (0.5, 1, 2, and 5 mg/mL) under visible light (left) and 365 nm UV light (right). (b) Statistic diagram of the diameter of the antibacterial zone of the antibacterial plate of *S. aureus* with VAN and VAN-CDs synthesized at different concentrations (0.5, 1, 2, and 5 mg/mL) under the same antibacterial concentration of 3 mg/mL. (c) TEM images of VAN-CDs prepared. (d) Size distribution diagram of VAN-CDs prepared. (e) Normalized fluorescence spectra of VAN-CDs at different excitation wavelengths from 310 to 390 nm. (f) Fluorescence attenuation curve of VAN-CDs. (g) XPS spectra of VAN-CDs: high-resolution XPS spectra of VAN-CDs include C 1s (h), O 1s (i), N 1s (j), and Cl 2p (k).

mixed solution were determined at an excitation wavelength of 360 nm.

The VAN-CDs solution (6 mg/mL) was mixed with different concentrations of the Sn^{4+} solution. The final concentration of each mixed solution was fixed as follows: VAN-CDs at 3 mg/mL with Sn^{4+} to final concentrations of 6, 7, 8, 9, 10, 20, 30, 40, 50, 60, 70, 80, 90, 100, 150, 200, 300, and 400 μM.

3. RESULTS AND DISCUSSION

Using a radiative power of 720 W, VAN-CDs were prepared at four reaction concentrations of 0.5, 1, 2, and 5 mg/mL for 20 min. The characteristics, fluorescence properties, and antibacterial activity of the VAN-CDs were studied in a preliminary manner (Figure 1). The prepared VAN-CDs emitted blue fluorescence under 365 nm UV light irradiation, whereas the VAN aqueous solution exhibited little fluorescence (Figure 1a

https://doi.org/10.1021/acsomega.3c05319
ACS Omega 2023, 8, 41469−41479

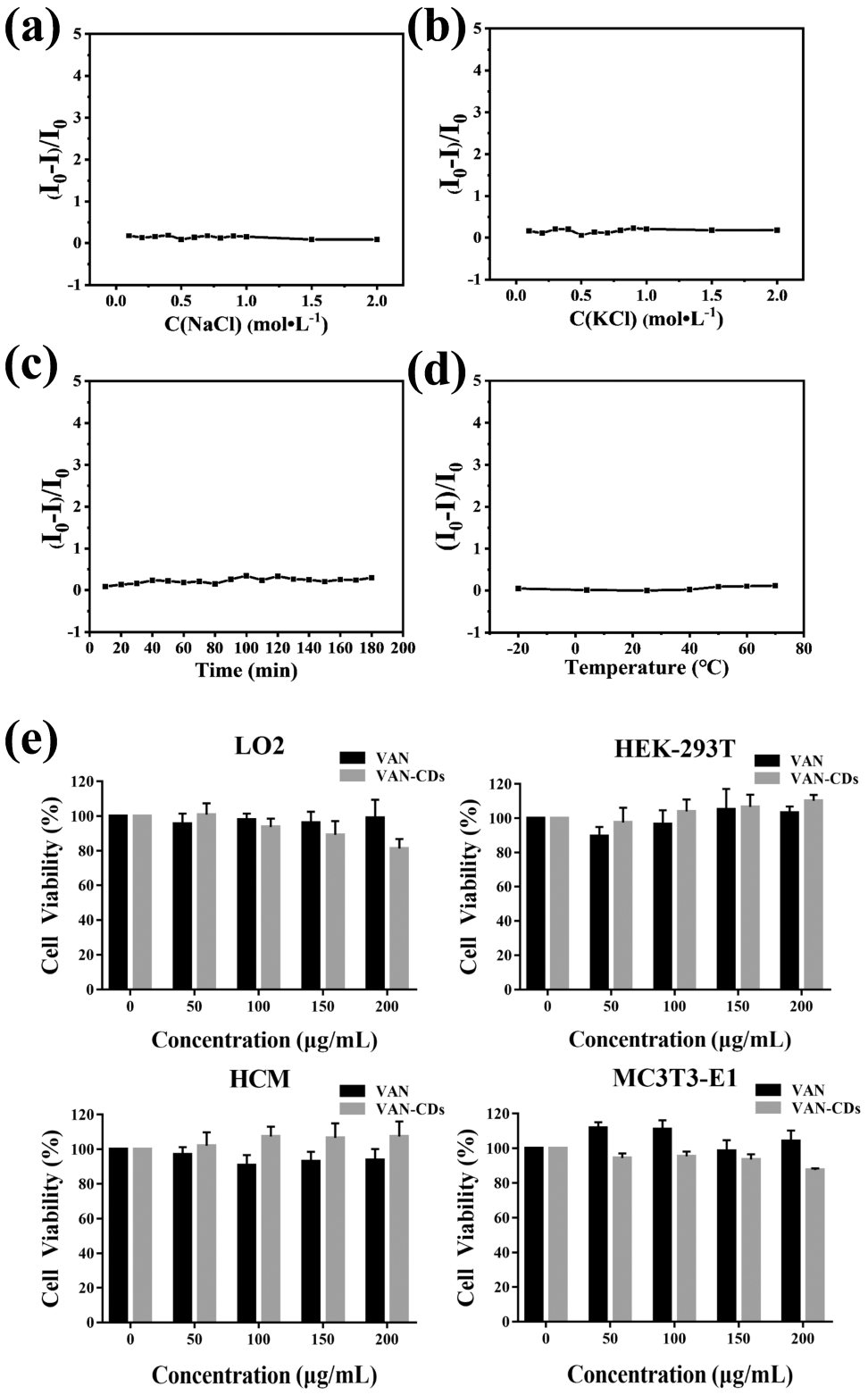

Figure 2. (a) The normalized chart of fluorescence intensity at the wavelength of 430 nm vs different concentrations of NaCl (0.1 0.2, 0.3, 0.4, 0.5, 0.6, 0.7, 0.8, 0.9, 1.0, 1.5, and 2.0 M) in the mixed solution of VAN-CDs. (b) The normalized chart of fluorescence intensity at the wavelength of 430 nm vs different concentrations of KCl (0.1, 0.2, 0.3, 0.4, 0.5, 0.6, 0.7, 0.8, 0.9, 1.0, 1.5, and 2.0 M) in the mixed solution of VAN-CDs. (c) The normalized chart of fluorescence intensity of VAN-CDs at the wavelength of 430 nm under UV light irradiation of 365 nm from 0−180 min. (d) The normalized chart of fluorescence intensity of VAN-CDs at the wavelength of 430 nm under different temperatures. (e) Cell viability of LO2, HEK293T, HCM, and MC3T3-E1 cells after incubation with VAN-CDs (0, 50, 100, 150, and 200 μg/mL) for 48 h.

and Figure S2a). Compared to VAN-CDs synthesized at 1, 2, and 5 mg/mL, the VAN-CDs solution synthesized at 0.5 mg/mL was much lighter under sunlight, and the fluorescence intensity was the weakest under 365 nm UV irradiation, which may be due to the low initial reaction concentration of VAN. The antibacterial effects of VAN and VAN-CDs synthesized at

https://doi.org/10.1021/acsomega.3c05319
ACS Omega 2023, 8, 41469−41479

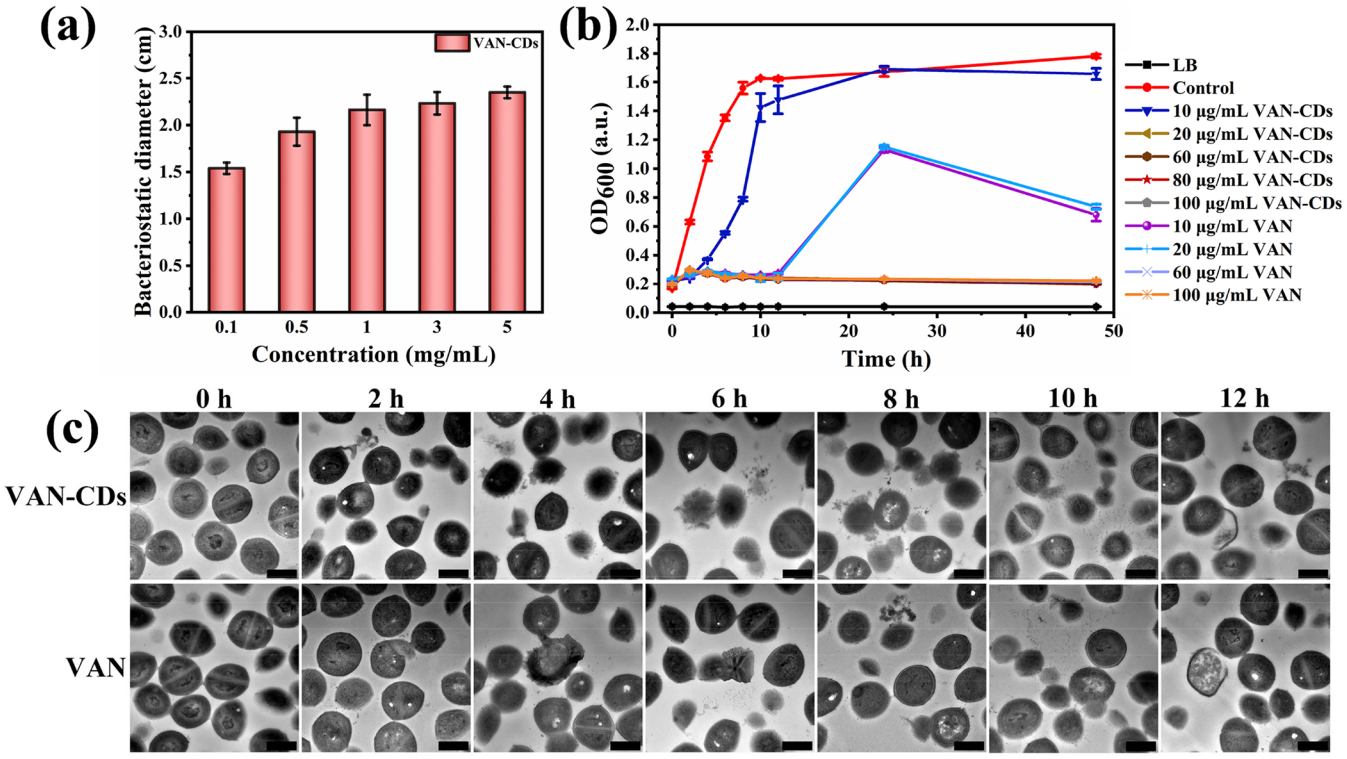

Figure 3. (a) Statistic chart of diameters of the bacteriostatic zone in the bacteriostatic plate at different concentrations of VAN-CDs. (b) Statistic diagram of OD value of LB medium, *S. aureus* (as Control), *S. aureus* cocultured with VAN-CDs at different concentrations (10, 20, 60, 80, and 100 μg/mL), and *S. aureus* cocultured with VAN at different concentrations (10, 20, 60, and 100 μg/mL), from 0 to 12 h. (c) TEM images of *S. aureus* treated with VAN-CDs (400 μg/mL) and VAN (400 μg/mL) for different times (0, 2, 4, 6, 8, 10, and 12 h), where the scale bars were 500 nm.

different concentrations (0.5, 1, 2, and 5 mg/mL) on *S. aureus* were investigated under the same antibacterial concentration of 3 mg/mL (Figure S1 and Figure 1b). At the same antibacterial concentration of 3 mg/mL, all of the VAN-CDs synthesized at different concentrations showed better antibacterial effects than VAN. Considering the following application of VAN-CDs for antibacterial and fluorescence detection, 1 mg/mL VAN-CDs was chosen for subsequent research.

The size of the VAN-CDs was uniform, with a diameter concentrated at approximately 0.899 ± 0.40 nm (Figure 1c,d). The VAN-CDs exhibited excitation-dependent fluorescence; when the optimal excitation wavelength was approximately 360 nm, the optimal emission wavelength of the VAN-CDs was approximately 430 nm (Figure 1e). Both VAN-CDs and VAN aqueous solutions exhibited strong UV absorption of the benzene ring at 280 nm (Figure S2b). The UV absorption intensity of the VAN-CDs was relatively high; this may be because following nanodot formation, the structural rigidity increased, the conjugated structures in the system were fixed, their vibration and rotation were limited, and the radiation transition increased. The fluorescence attenuation curve of the VAN-CDs was obtained by fitting the second-order attenuation exponential function (Figure 1f). Two fluorescence lifetimes (τ) were observed, implying that VAN-CDs possess two fluorescence centers (Table S1). The average lifetime and quantum yield of the VAN-CDs were 1.62 ns and 1.2%, respectively. According to previous studies, during the formation process of VAN-CDs, isolated specific sizes of sp^2 hybrid clusters may produce a blue emission band gap. Because of the electron−hole limitation and the surface of functional group doping, the VAN-CDs under the ultraviolet lamp emitted some blue fluorescence.[34,35] In the IR spectra, many chemical bonds of VAN were retained in the VAN-CDs system, including the benzene ring, C−N bond, C═C bond, C═O bond, O−H bond, and N−H bond (Figure S3). The X-ray photoelectron spectroscopy (XPS) spectrum (Figure 1g) shows that the VAN-CDs were composed of the following four elements: C, O, N, and Cl. High-resolution C 1s spectra showed that the VAN-CDs had absorption peaks at 284.8, 285.5, 286.5, and 288.4 eV, and the surface contained C−C/C═C, C−N, C−O, and C═O (Figure 1h). The 1s−OH spectra showed that the VAN-CDs had absorption peaks at 531.8 and 533.1 eV, corresponding to C═O and C−O, respectively (Figure 1i). In the N 1s spectrum, two peaks were observed at 400.2 and 402.2 eV, corresponding to C−N and $-NH_2$, respectively (Figure 1j). In the Cl 2p spectra, the VAN-CDs had absorption peaks at 197.9, 199.5, 200.8, and 202.4 eV, corresponding to Cl^{1-} $2p_{3/2}$, Cl^{1-} $2p_{1/2}$, C−Cl $2p_{3/2}$, and C−Cl $2p_{1/2}$, respectively (Figure 1k).

We next tested the fluorescence intensity changes of VAN-CDs under different concentrations of NaCl and KCl, long-term UV irradiation, and different temperatures to study their stability. When the NaCl concentration increased from 0 to 2.0 mol/L, the fluorescence intensity of VAN-CDs remained basically unchanged (Figure 2a and Figure S4a), and when the concentration of KCl was increased from 0 to 2.0 mol/L, the fluorescence intensity of VAN-CDs changed slightly (Figure 2b and Figure S4b). This proves that VAN-CDs have good salt ion stability. After 180 min of UV irradiation, the fluorescence intensity of the VAN-CDs system changed slightly (Figure 2c and Figure S4c), indicating good photobleaching resistance. Moreover, under different temperatures (−20, 4, 25, 37, 50, 60, and 70 °C), the fluorescence intensity of the VAN-CDs system

https://doi.org/10.1021/acsomega.3c05319
ACS Omega 2023, 8, 41469−41479

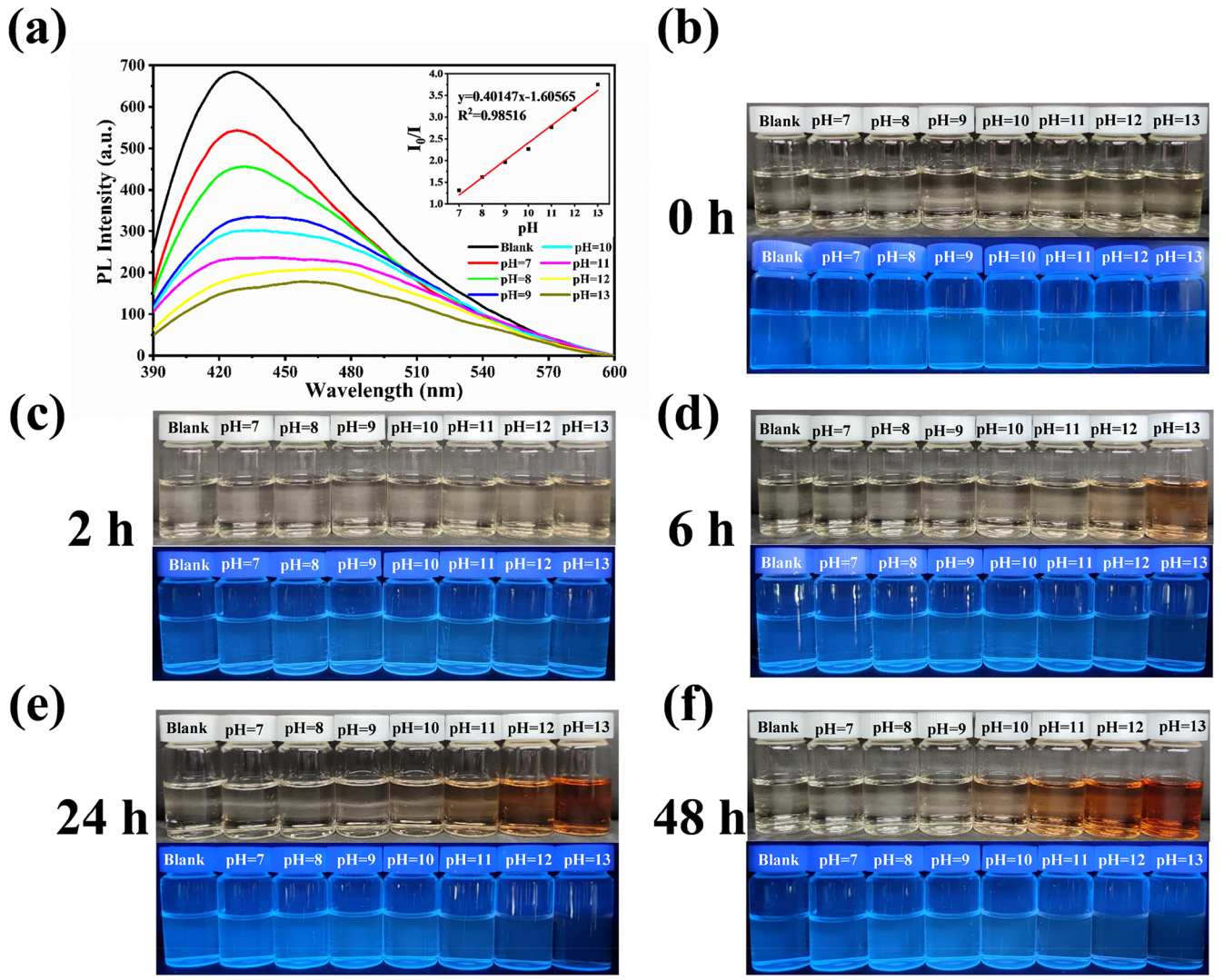

Figure 4. (a) Calculation diagram of fluorescent spectra of VAN-CDs solution (3 mg/mL) at different pH (7, 8, 9, 10, 11, 12, and 13) with the excitation wavelength of 360 nm. Inset was the corresponding calculated linear relationship between the fluorescence intensity at the wavelength of 430 nm of VAN-CDs solution vs pH (7, 8, 9, 10, 11, 12 and 13). Photos of VAN-CDs solution under visible light (above) and UV λ of 365 nm (below) at different pH value (7, 8, 9, 10, 11, 12, and 13) for (b) 0 h, (c) 2 h, (d) 6 h, (e) 24 h, and (f) 48 h, respectively.

changed slightly (Figure 2d and Figure S4d), indicating good temperature stability.

Low cytotoxicity is an important factor for VAN-CDs in many applications. The CCK-8 method was used to detect the impact of VAN-CDs on the viability of four normal cell types: mouse embryonic last precursor cells (MC3T3-E1), human embryonic kidney 293T cells (HEK 293T), human normal life cells (LO2), and human cardiac mycocells (HCM). After incubation with VAN-CDs (0, 50, 100, 150, and 200 μg/mL) for 48 h, all four types showed only a slight reduction in the viability (Figure 2e). The results showed that the prepared VAN-CDs had low biological toxicity.

As antibacterial performance is another important research objective of VAN-CDs (Figure 3), we used an *in vitro* antibacterial plate to investigate the antibacterial properties of VAN-CDs at different concentrations (0.1, 0.5, 1, 3, and 5 mg/mL) (Figure S5). As the concentration of the VAN-CDs solution increased, the diameter of the antibacterial zone on the agar plate gradually increased from approximately 1.54 to 2.35 cm (Figure 3a). The OD value changes of the following solutions were monitored from 0 to 48 h: LB culture medium, *S. aureus* (control group), *S. aureus* cultured with different concentrations of VAN (10, 20, 60, and 100 μg/mL), and *S. aureus* cultured with different concentrations of VAN-CDs (10, 20, 40, 60, 80, and 100 μg/mL) (Figure 3b). The OD value of the LB medium did not change over time, while the OD value of the *S. aureus* suspension rapidly increased to the plateau stage and slowly increased to the highest value with extension of the cultivation time (48 h). The OD value of the 10 μg/mL VAN-CDs group increased rapidly from 0 to 24 h, with a slower growth rate than that of the control group. At 48 h, the OD value was lower than that of the control group, indicating a weak inhibitory effect on *S. aureus*. The VAN group of 10 μg/mL showed an inhibitory effect on *S. aureus* within 12 h, but the inhibitory effect deteriorated afterward. Moreover, when the concentration of VAN-CDs was increased to 20 μg/mL, the OD value remained stable and very low, demonstrating its ability to continuously and effectively inhibit the growth of *S. aureus* from 0−48 h. The VAN group of 20 μg/mL had antibacterial effects similar to those of the VAN group of 10 μg/mL, which could not inhibit the growth of *S. aureus*. As the concentration of VAN-CDs increased to 60, 80, and 100 μg/mL, the antibacterial effect

https://doi.org/10.1021/acsomega.3c05319
ACS Omega 2023, 8, 41469−41479

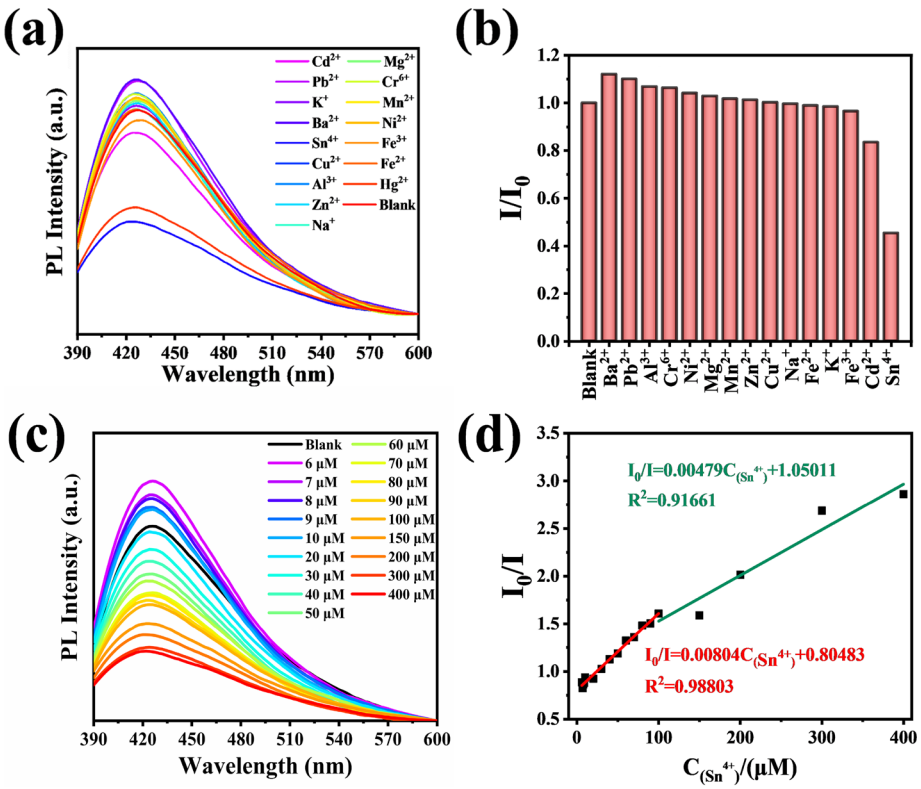

Figure 5. (a) Calculated fluorescent spectra and (b) corresponding calculated diagram of VAN-CDs solution (3 mg/mL) with different cations (Ba^{2+}, Pb^{2+}, Al^{3+}, Cr^{6+}, Ni^{2+}, Mg^{2+}, Mn^{2+}, Zn^{2+}, Cu^{2+}, Na^{+}, Fe^{2+}, K^{+}, Fe^{3+}, Cd^{2+}, Hg^{2+}, and Sn^{4+}) of the same concentration (100 μM). (c) Calculated fluorescent spectra and (d) corresponding calculated diagram of fluorescent intensity at the wavelength of 430 nm of VAN-CDs solution (3 mg/mL) with the increasing concentration (6−400 μM) of Sn^{4+}. The excitation wavelength was ∼360 nm.

was consistent. The inhibitory effect on *S. aureus* appeared when the VAN concentration was increased to 60 and 100 μg/mL. The results indicated that VAN-CDs at relatively low concentrations (20 μg/mL) had a better inhibitory effect on *S. aureus* than VAN.

TEM was used to observe the morphology of *S. aureus* after incubation with VAN and VAN-CDs for different times (0, 2, 4, 6, 8, 10, and 12 h) (Figure 3c). At 0 and 2 h, the cell walls of *S. aureus* in both the VAN and VAN-CDs groups were smooth, the growth status was good, and the morphology was intact. This suggested that in the early stage of incubation, VAN and VAN-CDs exerted little inhibitory effects or damage on *S. aureus*. As the incubation time was extended to 4 h, the cell walls of *S. aureus* in the two groups were clearly damaged, and the intracellular fluid began to seep outward. When the incubation time was prolonged to 12 h, *S. aureus* was more severely damaged, and the cell morphology was incomplete. As for VAN, it had a high affinity to the tail peptide structure D-Ala-D-Ala on the cell walls of Gram-positive bacteria, which presented a ligand−receptor-like interaction. It resulted in a large number of VAN gathering on the surface of the bacterial cell walls, inhibiting the formation of the bacterial cell walls via binding to them and then achieving the purpose of inhibiting bacteria.[36−39] Since the fabricated VAN-CDs retained many VAN structures and good antibacterial effects, combined with the observations from TEM images, it was inferred that the antibacterial mechanism of VAN-CDs was similar to that of VAN.

NaOH was used to adjust the pH of the VAN-CDs solution (3 mg/mL) to 7, 8, 9, 10, 11, 12, and 13 (Figure 4), before the fluorescence intensity was tested at room temperature (Figure 4a). The results showed that as the pH value of the solution increased, the fluorescence intensity of the VAN-CDs solution decreased. Moreover, fluorescence quenching occurred in VAN-CDs when the pH was 12−13. The fluorescence intensity of VAN-CDs was sensitive to pH in the range of 7−13, with a good linear relationship (insert in Figure 4a). As the surface of VAN-CDs is full of polar functional groups, such as carboxyl, hydroxyl, and carbonyl groups, dissociation of acidic groups and association of alkaline groups with H^{+} may occur in response to environmental pH changes.[40] Subsequently, the structure and fluorescent intensity of the VAN-CDs system may change. Next, the time-dependent sensitivity of the VAN-CDs solution to the pH was observed. From 0 to 48 h under visible light, the colors of the VAN-CDs solution at pH 7, 8, and 9 were consistent with those of the original VAN-CDs solution. The color of the VAN-CDs solution at pH 10, 11, 12, and 13 was faint yellow after 0 h. With increasing time, the color of the solution at pH 10, 11, 12, and 13 became darker, and at 48 h, the VAN-CD solution at pH 10, 11, 12, and 13 was light orange, orange, orange-red, and red, respectively (Figure 4). The darker the solution, the higher the pH value of the solution. Under the same conditions, the high pH value of the system can be directly confirmed according to the color of the solution. Interestingly, even if the color of the solution changed, the fluorescent intensity of the solution at each pH was rarely changed (Figure S6 and Figure S7). That is, the system can monitor pH values continuously and stably.

After mixing with different cations of 100 μM (Ba^{2+}, Pb^{2+}, Al^{3+}, Cr^{6+}, Ni^{2+}, Mg^{2+}, Mn^{2+}, Zn^{2+}, Cu^{2+}, Na^{+}, Fe^{2+}, K^{+}, Fe^{3+}, Cd^{2+}, Hg^{2+}, and Sn^{4+}), the fluorescence of each mixed VAN-CDs (3 mg/mL) solution was tested (Figure 5a,b). As can be seen in the diagrams, Ba^{2+}, Pb^{2+}, Al^{3+}, Cr^{6+}, and Ni^{2+} slightly increased the fluorescent intensity of VAN-CDs; Mg^{2+}, Mn^{2+}, Zn^{2+}, Cu^{2+},

https://doi.org/10.1021/acsomega.3c05319
ACS Omega 2023, 8, 41469−41479

Na^+, Fe^{2+}, K^+, and Fe^{3+} had little effect on the fluorescent intensity, and Cd^{2+} slightly reduced the fluorescent intensity. Similar to many previous reports, heavy ion Hg^{2+} quenched the fluorescence of VAN-CDs, indicating that VAN-CDs could be used to detect poison Hg^{2+} in the future.[41−43] Importantly, in contrast to previous studies, Sn^{4+} significantly quenched the fluorescence intensity of VAN-CDs, possibly because the conformation of the carbonyl and nitrogen atoms of VAN-CDs could chelate tin(IV) ions to induce fluorescence quenching. We next investigated the VAN-CDs fluorescent sensitivity over a larger concentration range (6−400 μM) of Sn^{4+} (Figure 5c). The results showed that with increasing concentration of Sn^{4+}, the fluorescent intensity of the VAN-CDs solution decreased linearly. Additionally, there were good linear relationships in the range of 6−100 and 100−400 μM, with linear equations of I_0/I = 0.00804 $C_{(Sn^{4+})}$ + 0.80483 (R^2 = 0.98803) and I_0/I = 0.00479 $C_{(Sn^{4+})}$ + 1.05011 (R^2 = 0.91661), respectively (Figure 5d). The VAN-CDs detection line of Sn^{4+} was approximately 5.2 μM. Meanwhile, the fluorescent properties of VAN-CDs with Sn^{2+} of different concentrations had been investigated. In Figure S8, Sn^{2+} showed a certain quenching effect on the fluorescence intensity of VAN-CDs, but it was obviously irregular. We speculated that Sn^{2+} was unstable and tended to be partially oxidized to Sn^{4+} in the mixed solution. It further proved that the fluorescent intensity of VAN-CDs had a particularly sensitive linear relationship with the increasing concentration of Sn^{4+}. We also discuss the quenching mechanism of Sn^{4+} on VAN-CDs by XPS spectra in Figure S9. It could be seen that Sn^{4+} combined the surface of VAN-CDs through Sn−O bonding. It may influence the surface properties of VAN-CDs as well as their fluorescent intensity.

4. CONCLUSIONS

In this study, VAN-CDs were rapidly synthesized via a one-step microwave method using an antibiotic, VAN as the sole precursor. The diameter of the VAN-CDs was concentrated at 0.899 ± 0.40 nm with a uniform size. When the optimal excitation wavelength was approximately 360 nm, the optimal emission wavelength of VAN-CDs was approximately 430 nm. The VAN-CDs retained some structural and antibacterial properties of VANs, although the results of antibacterial experiments showed that VAN-CDs had better antibacterial effects than VAN. The stability experiment demonstrated that VAN-CDs had good KCl/NaCl salt stability and photobleaching resistance. Moreover, the cytotoxicity experiments on LO2, HEK293T, HCM, and MC3T3-E1 cells showed that VAN-CDs had a lower biological toxicity. The fluorescence intensity of VAN-CDs was sensitive to pH in the range of 7−13 with a good linear relationship (R^2 = 0.98516). Furthermore, after mixing VAN-CDs with a series of different cations (Ba^{2+}, Pb^{2+}, Al^{3+}, Cr^{6+}, Ni^{2+}, Mg^{2+}, Mn^{2+}, Zn^{2+}, Cu^{2+}, Na^+, Fe^{2+}, K^+, Fe^{3+}, Cd^{2+}, Hg^{2+}, and Sn^{4+}) under the same conditions, only Hg^{2+} and Sn^{4+} quenched the fluorescence of VAN-CDs significantly. Further detailed experiments showed that VAN-CDs could specifically detect tin(IV) in the two ranges of 6−100 and 100−400 μM, with a good sensitive linear relationship. The detection line of VAN-CDs for Sn^{4+} was approximately 5.2 μM. The prepared multifunctional VAN-CDs have good application prospects in the fields of antibacterial, toxic Sn^{4+} detection, and pH-sensitive aspects.

ASSOCIATED CONTENT

Supporting Information

The Supporting Information is available free of charge at https://pubs.acs.org/doi/10.1021/acsomega.3c05319.

Copies of bacteriostatic plate experiments of VAN and serials of VAN-CDs, UV−vis spectrum, FT-IR spectrum, fluorescent life of VAN-CDs, UV−vis spectrum and FT-IR spectrum of VAN, stability investigation of VAN-CDs, fluorescent spectra and corresponding calculated diagram of VAN-CDs solutions at different pH, fluorescent spectra and corresponding calculated diagram of VAN-CDs solutions at different concentrations of Sn^{2+}, XPS spectra of VAN-CDs with Sn^{4+} (PDF)

AUTHOR INFORMATION

Corresponding Authors

Zhe Zhang − *Jilin Ginseng Academy, Changchun University of Chinese Medicine, Changchun 130117, People's Republic of China*; Email: zhangzhe@ccucm.edu.cn

Lei Zhao − *Jilin Ginseng Academy, Changchun University of Chinese Medicine, Changchun 130117, People's Republic of China*; Email: zhaolei@ccucm.edu.cn

Yu Zhao − *Jilin Ginseng Academy, Changchun University of Chinese Medicine, Changchun 130117, People's Republic of China*; orcid.org/0000-0003-2878-0929; Email: cnzhaoyu1972@126.com

Authors

Yingnan Jiang − *Jilin Ginseng Academy, Changchun University of Chinese Medicine, Changchun 130117, People's Republic of China*

Xinyu Zhao − *Jilin Ginseng Academy, Changchun University of Chinese Medicine, Changchun 130117, People's Republic of China*

Xuechun Zhou − *Jilin Ginseng Academy, Changchun University of Chinese Medicine, Changchun 130117, People's Republic of China*

Xiaoyu He − *Jilin Ginseng Academy, Changchun University of Chinese Medicine, Changchun 130117, People's Republic of China*

Lizhi Xiao − *Jilin Ginseng Academy, Changchun University of Chinese Medicine, Changchun 130117, People's Republic of China*

Jing Bai − *Jilin Jice Testing Technology Co., LTD., Changchun 130117, People's Republic of China*

Ying Yang − *Jilin Jice Testing Technology Co., LTD., Changchun 130117, People's Republic of China*

Quan Lin − *State Key Laboratory of Supramolecular Structure and Materials, College of Chemistry, Jilin University, Changchun 130012, People's Republic of China*

Complete contact information is available at: https://pubs.acs.org/10.1021/acsomega.3c05319

Author Contributions

‖These authors contributed to the work equally and should be regarded as cofirst author.

Notes

The authors declare no competing financial interest.

ACKNOWLEDGMENTS

This work was supported by the Natural Science Foundation of Jilin Province (YDZJ202201ZYTS562), Jilin Scientific and

Technological Development Program (20140622003JC and 202322), and the Jilin Province Development and Reform Commission (2014N155).

REFERENCES

(1) Jiang, Y.; Zhang, X.; Xiao, L.; Yan, R.; Xin, J.; Yin, C.; Jia, Y.; Zhao, Y.; Xiao, C.; Zhang, Z.; Song, W. Preparation of dual-emission polyurethane/carbon dots thermoresponsive composite films for colorimetric temperature sensing. *Carbon.* **2020**, *163*, 26−33.
(2) Sun, T.; Zhang, Y.; Yan, R.; Jiang, Y.; Zhao, Y. Preparation and Applications of Carbon-Based Fluorescent Nanothermometers. *Particle & Particle Systems Characterization.* **2021**, *38*, 2000261.
(3) Ehtesabi, H.; Hallaji, Z.; Najafi Nobar, S.; Bagheri, Z. Carbon dots with pH-responsive fluorescence: a review on synthesis and cell biological applications. *Microchimica Acta.* **2020**, *187*, 150.
(4) Song, W.; Zhang, H.; Liu, Y.; Ren, C.; Chen, H. A new fluorescence probing strategy for the detection of parathion-methyl based on N-doped carbon dots and methyl parathion hydrolase. *Chin. Chem. Lett.* **2017**, *28*, 1675−1680.
(5) Kong, B.; Zhu, A.; Ding, C.; Zhao, X.; Li, B.; Tian, Y. Carbon dot-based inorganic-organic nanosystem for two-photon imaging and biosensing of pH variation in living cells and tissues. *Adv. Mater.* **2012**, *24*, 5844−5848.
(6) Dong, H.; Liu, Y.; Zhao, Z.; Tan, X.; Managi, S. Carbon neutrality commitment for China: from vision to action. *Sustainability Science.* **2022**, *17*, 1741−1755.
(7) Zhao, Y.; Wang, X.; Mi, J.; Jiang, Y.; Wang, C. Metal Nanoclusters: Metal Nanoclusters-Based Ratiometric Fluorescent Probes from Design to Sensing Applications. *Particle & Particle Systems Characterization.* **2019**, *36*, 1970031.
(8) Fu, J.; Tan, X.; Li, Y.; Song, X. A nanosilica/exfoliated graphene composite film-modified electrode for sensitive detection of methyl parathion. *Chin. Chem. Lett.* **2016**, *27*, 1541−1546.
(9) Ju, B.; Nie, H.; Zhang, X.; Chen, Q.; Guo, X.; Xing, Z.; Li, M.; Zhang, X. Inorganic Salt Incorporated Solvothermal Synthesis of Multi-Color Carbon Dots, Emission Mechanism and Anti-bacterial Study. *ACS Applied Nano Materials.* **2018**, *1*, 6131−6138.
(10) Zhang, H.; Wei, R.; Chen, C.; Tuo, X.; Wang, X. A novel fluorescent epoxy resin for organophosphate pesticide detection. *Chin. Chem. Lett.* **2015**, *26*, 39−42.
(11) Thakur, M.; Pandey, S.; Mewada, A.; Patil, V.; Khade, M.; Goshi, E.; Sharon, M. Antibiotic Conjugated Fluorescent Carbon Dots as a Theranostic Agent for Controlled Drug Release, Bioimaging, and Enhanced Antimicrobial Activity. *Journal of Drug Delivery.* **2014**, *2014*, 282193.
(12) Wu, L.; Yang, Y.; Huang, L.; Zhong, Y.; Chen, Y.; Gao, Y.; Lin, L.; Lei, Y.; Liu, A. Levofloxacin-based carbon dots to enhance antibacterial activities and combat antibiotic resistance. *Carbon.* **2022**, *186*, 452−464.
(13) Li, P.; Liu, S.; Cao, W.; Zhang, G.; Yang, X.; Gong, X.; Xing, X. Low-toxicity carbon quantum dots derived from gentamicin sulfate to combat antibiotic resistance and eradicate mature biofilms. *Chemical Communications.* **2020**, *56*, 2316−2319.
(14) Luo, Q.; Qin, K.; Liu, F.; Zheng, X.; Ding, Y.; Zhang, C.; Xu, M.; Liu, X.; Wei, Y. Carbon dots derived from kanamycin sulfate with antibacterial activity and selectivity for Cr6+ detection. *Analyst.* **2021**, *146*, 1965−1972.
(15) Liang, J.; Li, W.; Chen, J.; Huang, X.; Liu, Y.; Zhang, X.; Shu, W.; Lei, B.; Zhang, H. Antibacterial Activity and Synergetic Mechanism of Carbon Dots against Gram-Positive and -Negative Bacteria. *ACS Applied Bio Materials.* **2021**, *4*, 6937−6945.
(16) Kuang, Y.; Song, M.; Zhou, X.; Mi, J.; Zhang, Z.; Liu, G.; Shen, Z.; Liu, Z.; Chen, C.; Wu, X.; Zhao, Y.; Yang, B.; Jiang, Y. Cefminox Sodium Carbon Nanodots for Treatment and Bacterial Detection of Bloodstream Infection. *Chemical Engineering Journal.* **2023**, *470*, 143988.
(17) Zhu, P.; Liu, Y.; Tang, Y.; Zhu, S.; Liu, X.; Yin, L.; Liu, Q.; Yu, Z.; Xu, Q.; Luo, D.; Wang, J. Bi-doped carbon quantum dots functionalized liposomes with fluorescence visualization imaging for tumor diagnosis and treatment. *Chin. Chem. Lett.* **2023**, 108689.
(18) Sun, Z.; Zhou, W.; Luo, J.; Fan, J.; Wu, Z.; Zhu, H.; Huang, J.; Zhang, X. High-efficient and pH-sensitive orange luminescence from silicon-doped carbon dots for information encryption and bio-imaging. *J. Colloid Interface Sci.* **2022**, *607*, 16−23.
(19) Yang, P.; Zhu, Z.; Zhang, T.; Zhang, W.; Chen, W.; Cao, Y.; Chen, M.; Zhou, X. Orange-Emissive Carbon Quantum Dots: Toward Application in Wound pH Monitoring Based on Colorimetric and Fluorescent Changing. *Small.* **2019**, *15*, No. e1902823.
(20) Zong, J.; Yang, X.; Trinchi, A.; Hardin, S.; Cole, I.; Zhu, Y.; Li, C.; Muster, T.; Wei, G. Carbon dots as fluorescent probes for "off-on" detection of Cu^{2+} and L-cysteine in aqueous solution. *Biosensors and Bioelectronics.* **2014**, *51*, 330−335.
(21) Ansi, V.; Renuka, N. Table sugar derived Carbon dot-a naked eye sensor for toxic Pb^{2+} ions. *Sensors and Actuators B: Chemical.* **2018**, *264*, 67−75.
(22) Sun, Y.; Wang, X.; Wang, C.; Tong, D.; Wu, Q.; Jiang, K.; Jiang, Y.; Wang, C.; Yang, M. Red emitting and highly stable carbon dots with dual response to pH values and ferric ions. *Microchimica Acta.* **2018**, *185*, 83−91.
(23) Deshwal, G.; Panjagari, N. Review on metal packaging: materials, forms, food applications, safety and recyclability. *Journal of Food Science and Technology.* **2020**, *57*, 2377−2392.
(24) Brulíkova, L.; Volná, T.; Hlavac, J. Bis-Rhodamine B System as a Tin Detector or Molecular Electronics Device. *ACS Omega.* **2020**, *5*, 9324−9333.
(25) Das, P.; Maruthapandi, M.; Saravanan, A.; Natan, M.; Jacobi, G.; Banin, E.; Gedanken, A. Carbon Dots for Heavy-Metal Sensing, pH-Sensitive Cargo Delivery, and Antibacterial Applications. *ACS Applied Nano Materials.* **2020**, *3*, 11777−11790.
(26) Ashworth, M.; Wilcox, G.; Higginson, R.; Heath, R.; Liu, C.; Mortimer, R. The effect of electroplating parameters and substrate material on tin whisker formation. *Microelectronics Reliability.* **2015**, *55*, 180−191.
(27) Liu, Y.; Niu, Y.; Ouyang, X.; Guo, C.; Han, P.; Zhou, R.; Heydari, A.; Zhou, Y.; Ikkala, O.; Tigranovich, G.; Xu, C.; Xu, Q. Progress of organic, inorganic redox flow battery and mechanism of electrode reaction. *Nano Research Energy.* **2023**, *2*, No. e9120081.
(28) Liu, J.; Wu, K.; Li, X.; Han, Y.; Xia, M. A water soluble fluorescent sensor for the reversible detection of tin(IV) ion and phosphate anion. *RSC Advances.* **2013**, *3*, 8924−8928.
(29) Du, J.; Zhao, M.; Huang, W.; Deng, Y.; He, Y. Visual colorimetric detection of tin(II) and nitrite using a molybdenum oxide nanomaterial-based three-input logic gate. *Analytical and Bioanalytical Chemistry.* **2018**, *410*, 4519−4526.
(30) Zhu, L.; Yang, J.; Wang, Q.; Zeng, L. Highly selective fluorescent probe for the detection of tin (IV) Ion. *J. Lumin.* **2014**, *148*, 161−164.
(31) Watanakunakorn, C. Mode of action and in-vitro activity of vancomycin. *J. Antimicrob. Chemother.* **1984**, *14*, 7−18.
(32) Turner, J.; Howe, R.; Wootton, M.; Bowker, K.; Holt, H.; Salisbury, V.; Bennett, P.; Walsh, T.; MacGowan, A. The activity of vancomycin against heterogeneous vancomycin-intermediate methicillin-resistant Staphylococcus aureus explored using an in vitro pharmacokinetic model. *J. Antimicrob. Chemother.* **2001**, *48*, 727−730.
(33) Phakatkar, A.; Firlar, E.; Alzate, L.; Song, B.; Narayanan, S.; Rojaee, R.; Foroozan, T.; Deivanayagam, R.; Banner, D.; Shahbazian-Yassar, R.; Shokuhfar, T. TEM Studies on Antibacterial Mechanisms of Black Phosphorous Nanosheets. *International Journal of Nanomedicine.* **2020**, *15*, 3071−3085.
(34) Qi, H.; Teng, M.; Liu, M.; Liu, S.; Li, J.; Yu, H.; Teng, C.; Huang, Z.; Liu, H.; Shao, Q.; Umar, A.; Ding, T.; Gao, Q.; Guo, Z. Biomass-derived nitrogen-doped carbon quantum dots: highly selective fluorescent probe for detecting Fe^{3+} ions and tetracyclines. *J. Colloid Interface Sci.* **2019**, *539*, 332−341.
(35) Chen, L.; Wu, C.; Du, P.; Feng, X.; Wu, P.; Cai, C. Electrolyzing synthesis of boron-doped graphene quantum dots for fluorescence determination of Fe^{3+} ions in water samples. *Talanta.* **2017**, *164*, 100−109.

https://doi.org/10.1021/acsomega.3c05319
ACS Omega 2023, 8, 41469−41479

(36) Dancer, R. J.; Try, A. C.; Sharman, G. J.; Williams, D. H. Binding of a vancomycin group antibiotic to a cell wall analogue from vancomycin-resistant bacteria. *Chemical Communications.* **1996**, *12*, 1445−1446.
(37) Gu, H.; Ho, P. L.; Tsang, K. W. T.; Wang, L.; Xu, B. Using biofunctional magnetic nanoparticles to capture vancomycin-resistant enterococci and other gram-positive bacteria at ultralow concentration. *J. Am. Chem. Soc.* **2003**, *125*, 15702−15703.
(38) Liu, T.; Tsai, K.; Wang, H.; Chen, Y.; Chen, Y.; Chao, Y.; Chang, H.; Lin, C.; Wang, J.; Wang, Y. Functionalized arrays of Raman-enhancing nanoparticles for capture and culture-free analysis of bacteria in human blood. *Nature Communications.* **2011**, *2*, 1−1.
(39) Zhong, D.; Zhuo, Y.; Feng, Y.; Yang, X. Employing carbon dots modified with vancomycin for assaying Gram-positive bacteria like Staphylococcus aureus. *Biosensors & Bioelectronics.* **2015**, *74*, 546−553.
(40) Liu, C.; Yang, M.; Hu, J.; Bao, L.; Tang, B.; Wei, X.; Zhao, J.; Jin, Z.; Luo, Q.; Pang, D. Quantitatively Switchable pH-Sensitive Photoluminescence of Carbon Nanodots. *Journal of Physical Chemistry Letters.* **2021**, *12*, 2727−2735.
(41) Li, Y.; Tang, L.; Zhu, C.; Liu, X.; Wang, X.; Liu, Y. Fluorescent and colorimetric assay for determination of Cu(II) and Hg(II) using AuNPs reduced and wrapped by carbon dots. *Microchim. Acta* **2022**, *189*, 10.
(42) Xu, J.; Wang, Z.; Liu, C.; Xu, Z.; Wang, N.; Cong, X.; Zhu, B. A highly selective colorimetric and long-wavelength fluorescent probe for the detection of Hg^{2+}. *Luminescence.* **2018**, *33*, 1122−1127.
(43) Liu, Z.; Jin, W.; Wang, F.; Li, T.; Nie, J.; Xiao, W.; Zhang, Q.; Zhang, Y. Ratiometric fluorescent sensing of Pb^{2+} and Hg^{2+} with two types of carbon dot nanohybrids synthesized from the same biomass. *Sensors and Actuators B: Chemical.* **2019**, *296*, 126698.

https://doi.org/10.1021/acsomega.3c05319
ACS Omega 2023, 8, 41469−41479